Characterizing chaos in systems subjected to parameter drift

Dániel Jánosi [*]

Institute for Theoretical Physics, Eötvös Loránd University, Pázmány Péter Sétány 1/A, H-1117 Budapest, Hungary

Tamás Tél [†]

Institute for Theoretical Physics, Eötvös Loránd University, Pázmány Péter Sétány 1/A, H-1117 Budapest, Hungary
and MTA-ELTE Theoretical Physics Research Group, Pázmány Péter Sétány 1/A, H-1117 Budapest, Hungary

To characterize chaos in systems subjected to parameter drift, where a number of traditional methods do not apply, we propose viable alternative approaches, both in the qualitative and quantitative sense. Qualitatively, following stable and unstable foliations is shown to be efficient, which are easy to approximate numerically, without relying on the need for the existence of an analog of hyperbolic periodic orbits. Chaos originates from a Smale horseshoe-like pattern of the foliations, the transverse intersections of which indicate a chaotic set changing in time. In dissipative cases, the unstable foliation is found to be part of the so-called snapshot attractor, but the chaotic set is not dense on it if regular time-dependent attractors also exist. In Hamiltonian cases stable and unstable foliations turn out to be not equivalent due to the lack of time-reversal symmetry. It is the unstable foliation, which is found to correlate with the so-called snapshot chaotic sea. The chaotic set appears to be locally dense in this sea, while tori with originally quasiperiodic character might break up, their motion becoming chaotic as time goes on. A quantity called ensemble-averaged pairwise distance evaluated in relation to unstable foliations is shown to be an appropriate tool to provide the instantaneous strength of time-dependent chaos.

I. INTRODUCTION

Although chaos theory might be seen to be completely understood by now, the field of systems subjected to parameter drift is yet to be fully explored. Here, basic methods of standard chaos cannot be applied, in particular, periodic orbits do not exist due to the lack of strict recurrences, thus the efficient tool of periodic orbit expansion [1] cannot be utilized. Furthermore, long-time limits are not meaningful since the system might become qualitatively different from the original one even after short times. As a consequence, the traditional definition of Lyapunov exponents [2] remains ill-defined. It is thus a basic question how to identify chaos in such systems. An entropy-based answer was given in [3]; here we address the question from the point of view of phase space structures, concentrating on time-dependent foliations and Smale horseshoes [4]. Additionally, a quantity describing the time-dependent sensitivity to initial conditions is proposed.

Some notable literature on drifting problems include tipping phenomena [5–7], aperiodically driven Hamiltonian systems [8], epidemics under changing vaccination coverage [9], advection in flows of changing intensity [10,11], as well as climate change (see, e.g., [12–17]). For a review, see [18].

The key element of traditional chaos (of undriven or periodically driven systems) is the existence of a Smale horseshoe [4]. This implies the intersection pattern of the interwoven unstable and stable manifolds of hyperbolic cycles. The set of transverse intersection points, called a chaotic saddle [2], is the fundamental set governing the dynamics. An equally well-known concept, used only rarely in the physics literature, is that of unstable and stable *foliations* [19–21]. They are defined as curves whose tangents point in the local stretching direction of the forward and backwards dynamics, respectively. A practical method to generate them is to scatter a large number of small balls in the phase space and iterate them forward or backward over long time intervals. These balls will deform into elongated ellipsoids whose increasing axes (still small) determine the local unstable or stable directions. Surfaces tangent to these directions constitute the foliations, and typically produce transverse intersections. As this algorithm implies, foliations are obtained *without* relying on the existence of hyperbolic orbits.

In systems subjected to parameter drift, both the analytic and numerical determination of distinguished hyperbolic orbits is hopeless, although, in special cases, perturbative results are available [18]. The unstable or stable manifold-based construction of horseshoes appears thus to be hopeless. We show here that the other, foliation-based approach is, by contrast, feasible, and leads to the construction of time-dependent foliations, which we call *snapshot foliations*. They can effectively be used to illustrate the existence of a time-dependent *snapshot horseshoe* and a *snapshot chaotic saddle*. Due to the impossibility of using long-time limits, all the results are, in a sense, approximate, but with the potential for improvement within certain limits.

Concerning dynamical instability we show, by extending recent results [8,18], that the so-called *ensemble-averaged pairwise distance* (EAPD) can be considered as a

---

[*]daniel.janosi@ttk.elte.hu
[†]tel@general.elte.hu

generalization of the concept of Lyapunov exponents since the local slope of this function can be interpreted as an instantaneous Lyapunov exponent.

II. MODEL

The understanding of drifting chaotic dynamics requires a strong revision of a number of traditional concepts, therefore, we stick throughout the paper to a single, but paradigmatic system: the Duffing equation [22,23], where the driving amplitude is chosen to linearly increase in time.

The dimensionless (scaled) equation of motion is

$$\ddot{x} = x - x^3 - 2\beta\dot{x} + (\varepsilon_0 + \alpha t)\cos\omega t, \quad t \geqslant 0, \quad (1)$$

where β is a damping constant and ω is the driving frequency. The driving amplitude is time dependent: ε_0 is its initial value and $\alpha > 0$ is the *rate* of the parameter drift. We define a *scenario*, starting at time $t = 0$ as the evolution of the driving amplitude set by parameters ε_0 and α. For convenience, we use a stroboscopic map by observing the system at integer multiples n of the period $T = 2\pi/\omega$. Besides the time of observation, n, we will also need an auxiliary time interval, denoted by k, also defined on the stroboscopic map. This will measure the time spent in the scenario *relative to n*.

We shall stick to scenarios with small driving amplitudes: $\varepsilon_{max} = \varepsilon_0 + \alpha t_{max} < 1$ where $t_{max} = n_{max}T$ denotes the longest time permitted by the validity of the model [24]. This restriction is kept to be able to compare the numerics with perturbative analytic expressions obtained in [18] for a few distinguished orbits. For our analysis, we choose $\varepsilon_{max} = 0.25$ and $\varepsilon_0 = 0.08$. Note that, although the driving amplitude is small, we are *not* in the adiabatic limit, which would imply $\alpha t_{max} \ll \varepsilon_0$. Instead, in the investigated cases the maximum change αt_{max} is comparable to ε_0.

III. DISSIPATIVE CASE

Equation (1) will be studied with $\beta = 0.01$ and $\omega = 1$, similarly to [18]. It is worth emphasizing that in the range $\varepsilon_0 \leqslant 0.25$ *no chaotic attractors exist* at all in the drift-free ($\alpha = 0$) case [18]. It was shown earlier [25] that any long-lasting chaoticity appearing in systems with parameter drift originates from chaotic transients [26] of the drift-free case.

A. Unstable foliation

The algorithm of following the evolution of small circles, although cumbersome, is applicable in drifting problems, as well. Furthermore, a transverse stable foliation is expected to exist as well, with an exponential convergence along it towards the unstable one. Thus, we can follow a simpler and more global approach, starting with a large number N of points distributed uniformly on a not infinitesimally small *interval* of length dl [27]. There is no need to specifically choose the orientation of this segment since images of it will quickly turn towards the instantaneous unstable direction, as a consequence of strong chaotic stretching.

To obtain the foliation belonging to discrete time instant n, the initialization has to be at $n - k \geqslant 0$ [28]. The result obtained with an initially vertical segment about phase-space
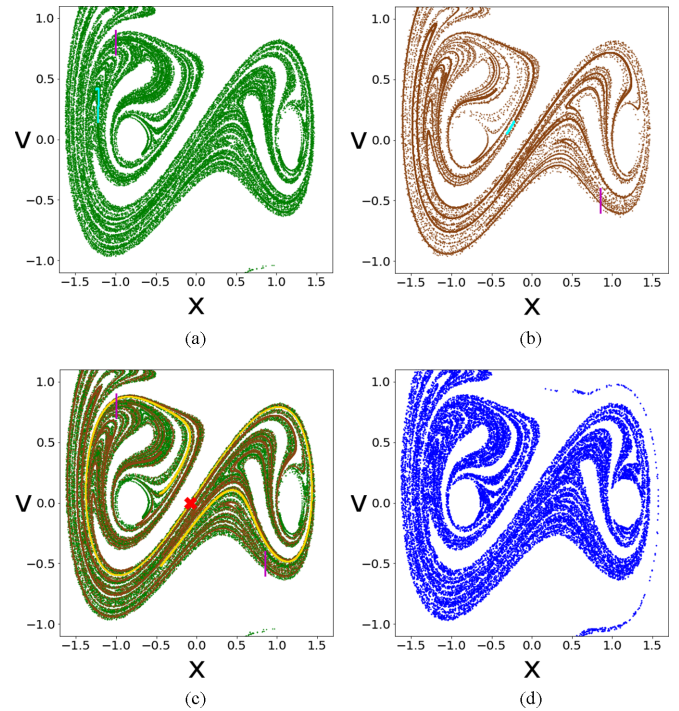

FIG. 1. Snapshot unstable foliation and its relation to the snapshot attractor in the scenario $\varepsilon_0 = 0.08$, $\alpha = 0.0005$ ($\beta = 0.01$, $\omega = 1$) at time $n = 25$. The filaments are generated from $N = 50\,000$ points on a vertical segment of length $dl = 0.2$ centered at (a) $(-1, 0.8)$ and (b) $(0.85, -0.5)$, marked by purple lines in both panels. The (a) green and (b) brown dots are the $k = 10$th images of the segments initiated at instant $n - k = 15$. The small light blue intervals are obtained from subintervals of length (a) $dl = 4 \times 10^{-4}$ and (b) $dl = 2 \times 10^{-3}$. (c) The snapshot unstable manifold (yellow) of the SHP (red cross), overlaid with the foliations of (a) and (b) at the same time instant. The unstable manifold was generated using $N = 50\,000$ points and with $dl = 5 \times 10^{-7}$. (d) The snapshot attractor (blue dots) at $n = 25$, evolved from an initially uniform distribution of $N = 40\,000$ points on a square of edge length 0.8 centered at the origin at time 0. Two disks of radius 0.2 are cut out from the shape of the ensemble about $(\pm 1, 0)$.

point $(-1, 0.8)$ after $k = 10$ steps is shown in Fig. 1(a) at instant $n = 25$. The first observation is that this is a fractal-like filamentation resembling chaotic foliations of traditional systems [29]. The small light blue segment is obtained from a tiny subinterval to illustrate that sufficiently short segments indicate directions touching the foliation tangentially. Figure 1(b) is an analogous picture where the initial segment is chosen to be centered at $(0.85, -0.5)$. Despite the considerable difference between the centers of the line segments, the resulting curves are *practically identical*. This is also the case with other positions and orientations. Not even with a larger value of k would one perceive any difference. We have, therefore, the right to call the union of all such curves an (approximate) *snapshot unstable foliation*.

Thanks to the smallness of ε_0 and α, as mentioned before, a distinguished hyperbolic trajectory was analytically determined in [18], within the framework of a perturbative approach. On the stroboscopic map, it is represented by a so-called snapshot hyperbolic point (SHP). The unstable manifold of this point can be determined in an analogous way,

just now the initial segment (not shown) is centered on the SHP and oriented in the local unstable direction. The result is shown in yellow in Fig. 1(c) overlaid with the foliations of Figs. 1(a) and 1(b). They all run parallel to each other, in a nearly indistinguishable way. The figure makes it plausible that the set of all unstable manifolds of all the SHPs, if known, would also coincide with the snapshot unstable foliation.

B. Snapshot attractor

The concepts adequate for the description of attractors in systems subjected to parameter drift are those of snapshot [30] or pullback [31] attractors. These concepts were used to understand a variety of time-dependent phenomena both in physics [32–34] and in relation to climate (see, e.g., [12,14,15,35,36]). We are going to stick to the snapshot interpretation since this remains applicable in the realm of Hamiltonian systems where the concept of pulling back is meaningless.

The determining feature of snapshot attractors is that they are generated by means of initially extended *ensembles* because individual time series are known [37] to be not representative. In addition, such attractors are *not ergodic* [38] due to the drift. After a convergence time, the distribution of the ensemble becomes *independent* of the initial one, the use of the term attractor is thus well founded. Under these conditions, the snapshot attractor is represented by the instantaneous shape and distribution of the ensemble.

Several snapshot attractors identified thus far exhibit a fractal appearance, and because of their analogy with traditional cases they were considered to represent chaotic dynamics [12,35,37]. Our results show that a refinement of this view is necessary, and propose to call snapshot attractors of fractal appearance *strange snapshot attractors*. We show that these need not be fully chaotic as they might incorporate components of regular dynamics as well.

The snapshot attractor of our Duffing system belonging to instant $n = 25$ is shown in Fig. 1(d) (the convergence time is about five periods) in blue. Due to the filamentary arrangement of the points, this is a strange snapshot attractor. A comparison of the blue dots with those of the foliation reveals that the numerically obtained *unstable foliation is an approximation of the snapshot attractor* (up to a few scattered points). This feature appears to be the generalization of the fact that traditional chaotic attractors are known to be the closures of the unstable manifolds of all the hyperbolic cycles, lying densely on the attractor [2].

C. Stable foliation

In analogy with the unstable case, the iteration runs over k periods *backward* in time from discrete time instant $n + k$ to n [39]. The result obtained with initial intervals around different points is shown in pink in Fig. 2(a) at instant $n = 25$. These, as well as the stable manifold of the SHP (not shown) all run parallel to each other. Remarkably, the shape and apparent fractality of the foliation would remain practically *unchanged* if a larger value of k were used, although it would extend more into ranges outside the region investigated in Fig. 2. There is thus a kind of convergence observed in the investigated area, and it appears that *the snapshot stable foli-*
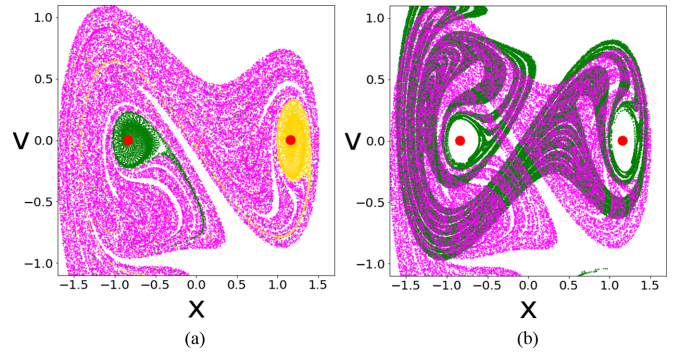

FIG. 2. The snapshot stable foliation, its relation to regular snapshot attractors, and a snapshot chaotic horseshoe at time $n = 25$ for the scenario used in Fig. 1. (a) The foliation is generated from three vertical segments of length $dl = 0.2$, each containing $N = 50\,000$ points, centered at $(-1, 0.8)$, $(0.25, 0)$, $(0.85, -0.5)$, initiated at time $n + k = 35$, obtained after $k = 10$ backward iterations, and marked by pink dots. The "basins of attraction" in green and yellow of the left and right SNPs (red dots), respectively, are overlaid with the stable foliation at time $n = 25$. The basins are obtained by generating the $k_b = 15$th inverse image of two circles of radius 0.2 about the SNPs, taken at the $n + k_b = 40$th iterate. (b) Snapshot chaotic horseshoe obtained by overlaying the unstable (stable) foliation of Fig. 1(c) and [Fig. 2(a)] marked with green (pink) initiated $k = 10$ steps earlier (later).

ation is fractal-like, leaving white bands free of any points of the foliation.

Traditionally, the stable foliation shades the basin of attraction of a chaotic attractor in a space filling way. This is in stark contrast to what we see here. To resolve this, we first need to mention that two time-dependent attracting points, called snapshot nodal points (SNPs), are known to exist about $x = \pm1$ whose perturbative locations are given in [18]. The generated strange snapshot attractor [Fig. 1(d)] thus certainly appears to *coexist* with these regular attractors. We can try constructing the "basins of attraction" of these SNPs. Since only finite-time properties can be investigated, most trajectories do not come really close to the regular attractors, therefore, we approximate by choosing two disks about the SNPs, and look for initial conditions which fall into them after some k_b number of forward iterations. Figure 2(a) also contains these basins superimposed on the snapshot stable foliation. From this, we conclude that the gaps in the foliation tend to be filled out with the "basins of attraction" of all existing SNPs.

D. Chaotic horseshoe and saddle

In drifting systems, one should pay attention to the fact that the snapshot foliations used for the horseshoe construction should belong to the same instant, n. This means that the unstable (stable) foliations should be initialized some k steps earlier (later), and then overlaid with each other [40]. This results in a *snapshot chaotic horseshoe*, while the set of intersection points between the foliations gives the *snapshot chaotic saddle*. This set inherits the properties of homoclinic and heteroclinic intersections in classical Smale horseshoes

since points of it come from chaos and go into chaos as our initial segments overlap with chaotic regimes [41].

The foliation-based snapshot horseshoe belonging to time instant $n = 25$ is shown in Fig. 2(b). One clearly sees that a large number of transverse intersections exist. It is surprising to see that the intersection points are *not dense along the unstable foliation*, in strong contrast to what is known about traditional chaotic attractors. Thus, the strange snapshot attractor supports only *transient chaos*. Note that, in parameter ranges where no SNPs exist, snapshot attractors might even be permanently chaotic, with a stable foliation expected to be space filling (Figs. S1 and S2 in [42]). Such attractors we call *chaotic snapshot attractors*.

The two disks cut out form the snapshot attractor in Fig. 1(d) contain a spiraling pattern towards the SNPs, as Fig. S3 of [42] illustrates. Thus, the strange snapshot attractor is not only partially (transiently) chaotic, it is partially fractal-like, as well. Without this cutting-out, one also sees that the strange snapshot attractor *includes* the regular snapshot attractors [42]. The unstable foliation also approaches the SNPs, albeit more slowly. We thus conclude that it is appropriate to consider the strange snapshot attractor a *single entity* containing both a chaotic component, the snapshot chaotic saddle, and regular ones, the SNPs, connected via the unstable foliation. Consistently, the union of the "basins of attraction" of chaos (i.e., the snapshot stable foliation) and of regular dynamics would fill the phase space, just as in drift-free cases.

IV. HAMILTONIAN CASE

Now we study the dissipation-free ($\beta = 0$) case of Eq. (1), corresponding to the Hamiltonian

$$H(p, x, t) = p^2/2 - x^2/2 + x^4/4 - x(\varepsilon_0 + \alpha t)\cos \omega t. \quad (2)$$

In the drift-free case, besides the Kolmogorov–Arnold–Moser (KAM) tori, macroscopic chaotic seas are found to exist in the *full* range of small driving amplitudes [8,18]. Under parameter drift, the divided nature of the phase space can only be followed if special initial subensembles are taken, corresponding to either KAM tori or chaotic seas of the drift-free ($\alpha = 0$) map. Following them under Eq. (2) we observe that the chaotic sea changes its shape, while the tori start to deform but remain closed curves until a certain point, where they break up and their dynamics become chaotic [8]. We call these ensembles *snapshot chaotic seas* and *snapshot tori*, respectively, while their joint ensemble is called the *snapshot phase portrait* [18]. Because of this structure, when applying the process described in the previous section to unstable or stable foliations belonging to time n, we need to consider small initial segments that are inside the snapshot chaotic sea at time $n \pm k$ as initial ensembles.

In Fig. 3 we show a Hamiltonian snapshot unstable [Fig. 3(a)] and stable [Fig. 3(b)] foliation, both belonging to $n = 25$ with $k = 20$, initiated from three initial segments fulfilling the above requirements. The foliations started from different initial intervals run parallel to each other in the Hamiltonian case as well. The perturbative SHP remains well defined here, and its unstable and stable manifolds (not shown) are also parallel to the respective foliations. In Fig. 3(c) we see the Hamiltonian snapshot chaotic horseshoe,
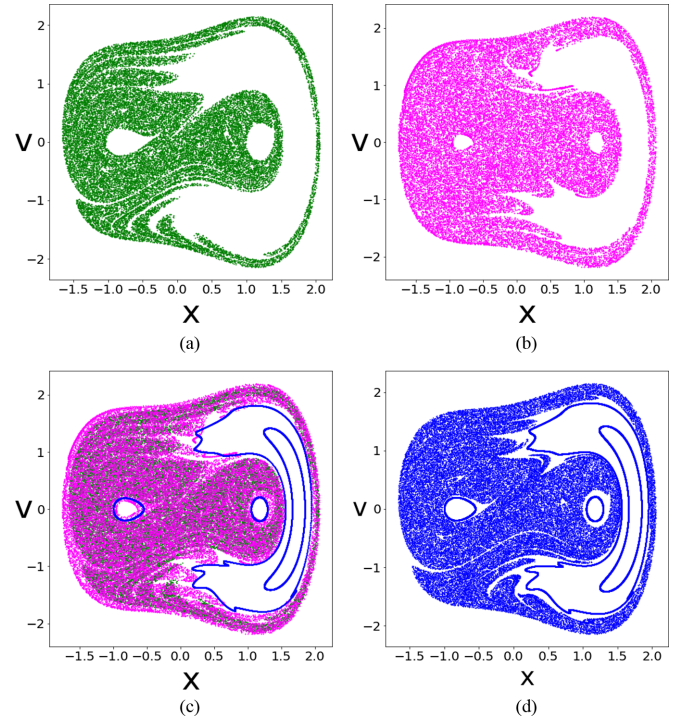

FIG. 3. Hamiltonian snapshot foliations ($\omega = 1$). (a) Unstable and (b) stable foliation in the same scenario as in Fig. 1 (with $\beta = 0$) belonging to $n = 25$ with $k = 20$. The initial segments are the same three as in Fig. 2 (but with $N = 10\,000$) for both foliations. (c) Snapshot chaotic horseshoe at time $n = 25$ with $k = 20$ obtained by overlaying the foliations in (a) and (b). The intersection points correspond to the snapshot chaotic saddle. (d) Snapshot phase portrait at $n = 25$ containing the same four snapshot tori as panel (c), as well as a snapshot chaotic sea initiated from the stationary phase portrait at $n = 0$. These are generated from the initial conditions $x_0 = -0.7, 0.95, 1.56, 1.65, v_0 = 0$ for the tori, and $x_0 = 0.1, v_0 = 0$ for the chaotic sea, respectively.

as well as some snapshot tori which survived the scenario as closed curves. Figure 3(d) shows the snapshot phase portrait at $n = 25$, with an extended snapshot chaotic sea and the same snapshot tori as in Fig. 3(c).

The first observation from Figs. 3(a) and 3(b) is that we can certainly make out an area which both foliations appear to densely shade, a trait that does *not* change with larger values of k or dl either. The unstable foliation possesses a perhaps more fragmented border, giving it a fractal-like appearance. It is striking to see that the two foliations do not shade the exact same area, in strong contrast to traditional cases.

Surprisingly, the stable foliation is of somewhat larger extension than the unstable one. The consequences of this can be clearly seen in Fig. 3(c): when constructing the horseshoe structure, one finds that, because the unstable foliation is *inside* the stable one, it appears that the intersection points, i.e., *the snapshot chaotic saddle coincides with the snapshot unstable foliation*.

Comparing the latter to the snapshot chaotic sea in Fig. 3(d), we can see that the two are *very similar*, and in a first approximation can be regarded identical. Thus here we can conclude that both the snapshot unstable foliation and the
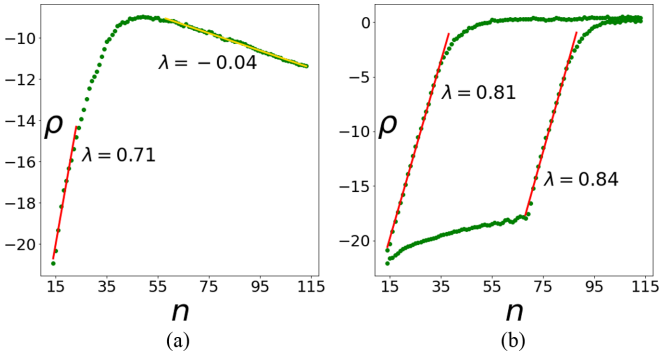
FIG. 4. EAPD curves of unstable foliations in the scenario $\varepsilon_0 = 0.08$, $\alpha = 0.0001$. The location of the initial vertical segment in both images is the same as in Fig. 1(a). The displayed (rounded-up) λ values are a few instantaneous Lyapunov exponents. (a) Dissipative case with $\beta = 0.01$. The dynamics is chaotic up to $n \approx 50$ with a positive but ever decreasing instantaneous Lyapunov exponent, followed by a phase of negative slope. (b) Hamiltonian case: The upper curve represents the unstable foliation. For completeness, on the lower curve we show the case of a snapshot torus initiated from the KAM torus of initial conditions $x_0 = -0.53$, $v_0 = 0$ started from $n = 15$.

snapshot chaotic sea are *locally space filling*, with fractal-like edges.

An interesting additional feature can be observed in Fig. 3(c). We see that parts of some surviving snapshot tori are *inside* the stable foliation. Such an overlap would be impossible in an autonomous map, but not here. The reason for this is that by our definition, the points of the stable foliation at n will be in a chaotic regime at $n + k$. This means, that the stable foliation intersecting with snapshot tori signals that those tori will have *broken up* by moment $n + k$: the motion of their points will have became chaotic-like [8], as will also be illustrated by Fig. 4(b).

V. MEASURE OF TIME-DEPENDENT CHAOS

Several different methods were suggested to quantify chaos in systems subjected to parameter drift [3,25,35,36]. As a particularly simple concept, we use here the one first suggested in [8] which enables an easy characterization of the time-dependent strength of chaos. The so-called *ensemble-averaged pairwise distance* (EAPD) is defined as

$$\rho_n = \langle \ln r_n \rangle, \tag{3}$$

where the average is taken over an *ensemble* of trajectories for which r_n is the distance between a test particle and an ensemble member at discrete times n, being at a distance r_0 to each other initially. In earlier cases this ensemble was chosen to be that of a snapshot torus [8] or a snapshot attractor [18]. The slope of the EAPD curve can be considered as an instantaneous Lyapunov exponent λ, a quantity that can be used to describe time-dependent chaos.

Here we extend this concept to *foliations*, and take as ensemble the N initial conditions along the line segments of length dl used earlier. The results for the unstable foliation is shown in Fig. 4. To have a large number of data points, a slower scenario is taken than the one used so far. The

evaluation of the EAPD starts with the initialization of the foliation at $n = 15$ and goes until $n + k = 115$ while $\alpha = 0.0001$, meaning that the scanned amplitude range is similar to that of the previous scenario. The r_0 initial distance between point pairs is $\sqrt{2} \times 10^{-10}$, i.e., we add 10^{-10} in both directions to the coordinates of the ensemble members.

Figure 4(a) shows a dissipative case. We see that the motion is chaotic over several periods, but at around $n = 50$ the slope becomes zero, chaos disappears from the system. As mentioned before, the unstable foliation approaches the SNPs, and in this scenario it does this fast enough to turn the average motion from chaotic to regular, as evidenced by the small negative slope. The shape of the curves has little dependence on the location of the initial segment. If we follow the EAPD of the ensemble of the strange snapshot attractor, the curve would have a similar shape (see Fig. S4 in [42]).

In Fig. 4(b) we see a Hamiltonian case. The upper curve again represents the unstable foliation, and in this case it levels off around 0, indicating a scattering of all points in a macroscopic phase space region, i.e., pronounced chaos. Evaluating the EAPD for the snapshot chaotic sea started from $n = 15$, we would get a qualitatively similar curve (not shown). The lower curve represents a snapshot torus that breaks up during the scenario, demonstrating that this is indeed a process that turns regular motion into chaotic, with a finite instantaneous Lyapunov exponent, which is found to be similar to that of the snapshot chaotic sea at the moment of the break-up ($n \approx 70$), see Fig. S5 in [42].

VI. CONCLUSION

We have shown that chaos in systems subjected to parameter drift is best described using approximate unstable or stable foliations, which are easy to obtain numerically. These constitute a Smale horseshoe structure, as well as a chaotic saddle, which govern the details of time-dependent chaotic dynamics. It is the unstable foliation which turns out to be strongly related to the relevant chaotic sets. The time dependence of the strength of chaos can be effectively followed by evaluating the EAPD. Although our illustrative example is low-dimensional and periodically driven, most of the ideas presented here apply in nondriven cases, as well. In [18,43] the dynamics of the decay caused by dissipation was studied in problems lacking any energy input, while in [27] nondriven conservative motion with time-dependent parameters was investigated on a Poincaré map. The ideas can also be generalized to higher-dimensional systems. Foliations can be generated by iterating small hypersurfaces forward and backward, which then possess common points, the analogs of snapshot chaotic saddles. The evaluation of the EAPD is straightforward for high-dimensional chaotic sets and can, in principle, be worked out in large-scale climate models as well.

ACKNOWLEDGMENTS

[1] P. Cvitanovic, R. Artuso, R. Mainieri, G. Tanner, and G. Vattay, *Chaos: Classical and Quantum*, available at ChaosBook.org, version 16.4 (2020).

[2] E. Ott, *Chaos in Dynamical Systems* (Cambridge University Press, Cambridge, England, 1993).

[3] B. Hunt and E. Ott, Chaos **25**, 097618 (2015).

[4] S. Smale, Bull. Amer. Math. Soc. **73**, 747 (1967).

[5] B. Kaszás, U. Feudel, and T. Tél, Sci. Rep. **9**, 8654 (2019).

[6] S. Pierini and M. Ghil, Sci. Rep. **11**, 11126 (2021).

[7] S. Wieczorek, X. Chun, and P. Ashwin, arXiv:2111.15497.

[8] D. Jánosi and T. Tél, Chaos **29**, 121105 (2019).

[9] T. Kovács, J. R. Soc. Interface **17**, 20200648 (2020).

[10] G. Haller, Annu. Rev. Fluid Mech. **47**, 137 (2015).

[11] R. D. Vilela, J. Phys. Complex. **2**, 035013 (2021).

[12] M. D. Chekroun, E. Simonnet, and M. Ghil, Physica D **240**, 1685 (2011).

[13] C. Deser, Earth's Future **8**, E2020EF110854 (2020).

[14] M. Ghil, M. D. Chekroun, and E. Simonnet, Physica D **237**, 2111 (2008).

[15] M. Ghil and V. Lucarini, Rev. Mod. Phys. **92**, 035002 (2020).

[16] T. Haszpra, M. Herein, and T. Bódai, Earth Syst. Dynam. **11**, 267 (2020).

[17] D. Patel, D. Canaday, M. Girwan, A. Pomerance, and E. Ott, Chaos **31**, 033149 (2021).

[18] D. Jánosi, Gy. Károlyi, and T. Tél, Nonlinear Dynamics **106**, 2781 (2021).

[19] Y. G. Sinai, Russ. Math. Surv. **25**, 137 (1970).

[20] Y. B. Pesin and Y. G. Sinai, Ergod. Theor. Dyn. Syst. **2**, 417 (1982).

[21] D. Ruelle, *Elements of Differentiable Dynamics and Bifurcation Theory* (Elsevier, Amsterdam, 1989).

[22] J. Argyris, G. Faust, M. Haase, and R. Friedrich, *An Exploration of Dynamical Systems and Chaos* (Springer, New York, 2015).

[23] A. Hadjighasem, M. Farazmand, and G. Haller, Nonlinear Dynamics **73**, 689 (2013).

[24] This immediately implies a constraint as $k \leqslant n_{max}$.

[25] B. Kaszás, U. Feudel, and T. Tél, Phys. Rev. E **94**, 062221 (2016).

[26] Y.-C. Lai and T. Tél, *Transient Chaos* (Springer, New York, 2011).

[27] A naive precursor to this approach was illustrated for a discrete-time conservative map in D. Jánosi and T. Tél, Chaos **31**, 033142 (2021).

[28] Because the scenario is defined in the time range $t \geqslant 0$, $k \leqslant n$ follows.

[29] The fractal appearance here (and everywhere else) is characteristic to large scales only as a true fractal feature would require an infinite-time integration.

[30] F. J. Romeiras, C. Grebogi, and E. Ott, Phys. Rev. A **41**, 784 (1990).

[31] P. E. Kloeden, J. Differ. Equations Appl. **6**, 33 (2000).

[32] Y.-C. Lai, Phys. Rev. E **60**, 1558 (1999).

[33] R. Serquina, Y.-C. Lai, and Q. Chen, Phys. Rev. E **77**, 026208 (2008).

[34] M. Vincze, I. Dan Borcia, and U. Harlander, Sci. Rep. **7**, 254 (2017).

[35] S. Pierini, M. Ghil, and M. D. Chekroun, J. Climate **29**, 4185 (2016).

[36] S. Pierini, D. Chekroun, and M. Ghil, Nonlinear Proc. Geophysics **25**, 671 (2018).

[37] T. Tél, T. Bódai, G. Drótos, T. Haszpra, M. Herein, B. Kaszás, and M. Vincze, J. Stat. Phys. **179**, 1496 (2020).

[38] G. Drótos, T. Bódai, and T. Tél, Phys. Rev. E **94**, 022214 (2016).

[39] For $n > n_{max}/2$, the restriction $k \leqslant n$ is replaced by $k \leqslant n_{max} - n$.

[40] The choice of the same k for both foliations is for convenience.

[41] Approximate snapshot saddles were identified earlier based on manifolds of cycle points in [8,18] and by means of the sprinkler method in [25,26].

[42] See Supplemental Material at http://link.aps.org/supplemental/10.1103/PhysRevE.105.L062202 for extra figures illustrating some aspects not detailed in the text.

[43] Gy. Károlyi and T. Tél, J. Phys. Complex. **2**, 035001 (2021).